Preprint Cambridge Centre for Computational Chemical Engineering ISSN 1473 – 4273

Efficient simulation and auto-calibration of soot particle processes in Diesel engines

Shaohua Wu [1], Jethro Akroyd [2,3], Sebastian Mosbach [2,3],
George Brownbridge [4], Owen Parry [4], Vivian Page [6],
Wenming Yang [1], Markus Kraft [2,3,5,*]

released: 23 June 2019

[1] Department of Mechanical Engineering
National University of Singapore
Engineering Block EA
Engineering Drive 1
Singapore, 117576

[2] Department of Chemical Engineering
and Biotechnology
University of Cambridge
West Cambridge Site
Philippa Fawcett Drive
Cambridge, CB3 0AS
United Kingdom

[3] Cambridge Centre for Advanced Research
and Education in Singapore (CARES)
CREATE Tower
1 Create Way
Singapore 138602

[4] CMCL Innovations
Sheraton House
Cambridge, CB3 0AX
United Kingdom

[5] School of Chemical and
Biomedical Engineering
Nanyang Technological University
62 Nanyang Drive
Singapore, 637459

[6] Industrial Power Systems Division
Caterpillar UK
Peterborough
United Kingdom

Preprint No. 231

Keywords: Diesel engine, soot, calibration.

Edited by
Computational Modelling Group
Department of Chemical Engineering and Biotechnology
University of Cambridge
West Cambridge Site
Philippa Fawcett Drive
Cambridge CB3 0AS
United Kingdom

Fax: + 44 (0)1223 334796
E-Mail: c4e@cam.ac.uk
World Wide Web: https://como.ceb.cam.ac.uk/

Abstract

Parameters describing soot particle processes are generally derived from a limited number of experimental studies. These parameters then have to be carefully calibrated for different operating conditions in internal combustion engine applications. This paper presents an innovative calibration procedure for soot simulation in Diesel engines. A Diesel engine is simulated using the Stochastic Reactor Model (SRM) engine code, which is implemented with the Moment Projection Method (MPM) for handling the soot particle dynamics. The main advantage of the engine-soot model is its low computational cost. The model is then coupled with an advanced statistical toolkit, Model Development Suite (MoDS), where the Hooke-Jeeves algorithm is adopted to calibrate seven soot model parameters automatically based on the measurement data. The ability of the integrated SRM-MoDS code for soot model calibration is evaluated by simulating the soot formation and oxidation processes in a heavy-duty Diesel engine which is operated under 18 different conditions. Results suggest that the integrated code is able to calibrate the soot model parameters effectively. A significant improvement in the match between the simulation results and experimental soot emission is obtained after calibration.

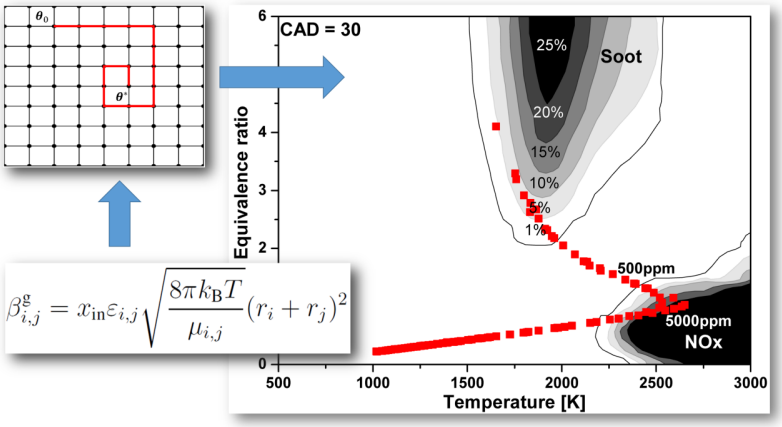

Highlights:

- The Moment Projection Method is used to simulate soot formation in engines.
- Seven soot model parameters are calibrated through Hooke-Jeeves optimisation.
- Measurements from a heavy-duty Diesel engine at 18 operating conditions are used for calibration.
- Significantly improved agreement between model and experiment is obtained.

Contents

1 Introduction

Compared with gasoline engines, the merits of Diesel engines are lower fuel consumption and higher thermal efficiency [6, 7]. Diesel engines are therefore heavily relied upon for power generation, seaborne and land transport for freight as well as for passenger cars. However, due to the existence of rich high temperature zones leading to fuel pyrolysis, Diesel engines tend to produce more soot and other particulate matter (PM) in the exhaust gas which challenges its viability as more stringent emissions standards have been imposed [11, 12, 25, 50]. In order to improve our understanding of the soot formation and oxidation mechanisms and to meet the demand for cleaner combustion strategies, modelling and simulation of soot formation and oxidation in Diesel engines are of increasing importance.

The formation and oxidation of soot is a rather sophisticated physical and chemical process involving gas-phase chemistry, heterogeneous reactions on the particle surface and particle dynamics depending on a wide range of parameters [7, 14, 20, 40, 44]. The major processes considered important for soot formation in Diesel engines include: inception, *i.e.* formation of the primary soot particles through collision of two polycyclic aromatic hydrocarbon (PAH) molecules [49]; condensation, *i.e.* deposition of the PAH molecule on the soot surface leading to soot mass growth [33]; coagulation, *i.e.* formation of large soot particles due to collision and sticking among the small ones [23, 24, 36]; surface growth, *i.e.* increase of soot mass following the hydrogen-abstraction and acetylene-addition (HACA) mechanism [16], and oxidation where the soot particle is oxidised through heterogeneous reactions with molecular oxygen and hydroxyl radicals [16]. The evolution of the soot particle size distribution (PSD) can be modeled by using population balance equations (PBEs) which are in mathematics a set of partial differential equations [48]. However, parameters describing these soot process rates are derived from a limited number of experimental or theoretical studies. There is a lack of consensus within the literature in terms of these parameters and the uncertainty ranges. Therefore, the soot model parameters usually have to be properly calibrated for different engine geometries and operating conditions.

The purpose of calibration is to determine the model parameters to achieve the smallest difference between the experimental measurements and the numerical simulation results with the minimum consumption of computation time. Manual calibration is time-consuming, impractical and cannot always give the optimal results. To realise efficient model-based engineering, it is vital to combine the physical-chemical model with advanced optimisation method to achieve the auto-calibration of the model parameters. Pasternak et al. [43] present a self-calibration model for Diesel engine simulation. The model consists of a stochastic reactor model (SRM) for Diesel engine in-cylinder processes simulations and a package of optimisation algorithms (OPAL) for various optimisation problems. The genetic algorithms (GA) were adopted to determine the model parameters for calibration against the measured in-cylinder pressure history and engine-out emissions, including nitrogen oxides and unburned hydrocarbons. It has been shown that the presented approach is able to efficiently calibrate the Diesel engine model. A higher calibration accuracy is achieved compared to the manual calibration. Niu et al. [41] propose a combination of GA and the ant colony algorithms for calibrating the com-

bustion and heat transfer parameters including radiation coefficient, the combustion speed and terminal angle. This new approach has been shown to satisfy the required accuracy with a reduced number of simulation times. Prah et al. [47] propose a Hybrid Calibration Method (HCM) for internal combustion engine (ICE) simulation. This method consists of two steps. The first step comprises the determination of calibration parameters for ICE sub-systems based on the direct search procedure. In the second step, calibration is performed with a reduced number of calibration parameters for the entire ICE simulation. The main advantage of HCM is its ability for the calibration of a large number of tuning parameters in a robust, repeatable and time-efficient manner.

The current literature on the engine model calibration is largely targeted at the engine in-cylinder pressure. Very little is focused on soot emissions. In the few publications [29, 42] where the soot emission is the calibration target, the adopted soot models are restricted to over-simplified empirical ones [17, 18]. The main advantage of these empirical soot models is the low computational cost. However, they do not account for the detailed soot particle dynamics. As a result, limited information on the soot formation and oxidation processes can be provided. By contrast, the detailed soot model is able to provide a deep insight into the soot particle dynamics. The problem is that the PBEs describing the soot particle processes usually take lots of computational resources, making the calibration highly time-consuming given the fact that usually multiple simulation times are needed to complete the calibration process. An efficient engine-soot code is therefore desired for calibration of the detailed soot model parameters. Generally, there exist three approaches to handle the soot PBEs: stochastic method [4, 30], sectional method [1, 27, 28] or method of moments (MOM) [15, 32, 34]. The stochastic method and sectional method are accurate and able to provide the detailed soot PSD but suffer from a high computational cost. MOM is much superior to other methods in terms of computational efficiency. With MOM, the soot PBEs are transformed into a set of moment equations and only a few lower-order moments are solved for, thus reducing the computational cost significantly. However, MOM suffers from some closure problems arising from the application of realistic collision kernels and particle depletion due to oxidation. Over the last three decades, numerous moment methods have been proposed [10, 15, 31, 32, 34, 40, 57] trying to handle these problems. Among them, the Moment Projection Method (MPM) [54, 55] is very promising, having been shown to be able to handle all particle processes with satisfactory accuracy.

The aim of this paper is to present an efficient calibration procedure for soot simulation in Diesel engines. To achieve that goal, the Stochastic Reactor Model (SRM) engine code [13, 26, 29, 37, 38, 42, 52] is used to simulate the combustion process inside Diesel engines. The Moment Projection Method is implemented to handle the soot particle dynamics. The SRM code is then coupled with the Model Development Suite (MoDS) [8, 39] where a direct search algorithm is adopted to calibrate the soot model parameters automatically based on the measured soot emission data at different operating conditions.

The paper is structured as follows. In the next section, the engine and soot models are presented. The incorporation of the Moment Projection Method into the SRM framework is explained followed by a brief description of the calibration algorithm. In section 3, the performance of the integrated code for calibration of soot model parameters is tested

by simulating a four-cylinder heavy-duty Diesel engine operated under 18 different conditions which cover a wide range of soot emissions. Finally, some key conclusions are summarised.

2 Model description

2.1 Engine model

The Stochastic Reactor Model (SRM) engine code is a spatially zero dimensional model for physical and chemical processes, which is applicable for simulations of in-cylinder combustion processes [26, 38]. The model is inspired by the Probability Density Function (PDF) transport methods [45]. It employs detailed chemical kinetics and possesses submodels for heat transfer, turbulent mixing, piston movement, and fuel injection [29, 52]. An important concept in the SRM is the so-called "stochastic particle" which represents a point in phase-space for the local scalar variables such as species concentrations, temperature, and pressure [37]. The engine cylinder charge can be split into an ensemble of stochastic particles to represent the distribution of these variables. These stochastic particles can mix with each other and exchange heat with the cylinder walls [13]. The number of stochastic particles determines the precision of the physical predictions. Higher accuracy is achieved with a larger number of stochastic particles but at the expense of computational cost. Usually 100 stochastic particles are sufficient for engine simulations.

2.2 Soot model

Within each stochastic particle, the soot model proposed by [2, 3] is adopted in this work to describe the soot formation and oxidation processes. The soot is modelled as a population of spherical particles composed of merely carbon atoms. The physical and chemical processes considered to be important for the formation of soot particles are inception, coagulation, condensation, surface growth, and oxidation. The detailed description of these processes can be found in [2, 3]. Here we only focus on the soot reaction kernels. We have introduced a set of multipliers which are applied to these kernels so that the soot reaction rates can be calibrated against the experimental soot emissions.

For inception, the reaction rate is expressed by using a collision efficiency model with the collision kernel given as:

$$\beta_{i,j}^{\mathrm{g}} = x_{\mathrm{in}} \varepsilon_{i,j} \sqrt{\frac{8\pi k_{\mathrm{B}} T}{\mu_{i,j}}} (r_i + r_j)^2. \tag{1}$$

$\varepsilon_{i,j}$ is a size-dependent enhancement factor due to attractive or repulsive inter-particle forces. k_{B} is the Boltzmann constant, T is the temperature, $\mu_{i,j}$ is the reduced mass of the collision species, and r_i is the radius of the species of size i. x_{in} is the multiplier introduced to tune the soot inception rate.

Table 1: *Soot surface reactions. The rate parameters are taken from [2].*

No.	Reaction	$k = AT^n\exp(-E/RT)$ A [$cm^3/mol/s$]	n [-]	E [kcal/mol]	Multiplier
S1	$C^i_{\text{soot-H}} + H \rightleftharpoons C^i_{\text{soot-}} + H_2$	4.2×10^{13}		13.0	-
		3.9×10^{12}		11.0	-
S2	$C^i_{\text{soot-H}} + OH \rightleftharpoons C^i_{\text{soot-*}} + H_2O$	1.0×10^{10}	0.734	1.43	-
		3.7×10^{8}	1.139	17.1	-
S3	$C^i_{\text{soot-*}} + H \rightarrow C^i_{\text{soot}}$	2.0×10^{13}			-
S4	$C^i_{\text{soot-*}} + C_2H_2 \rightarrow C^{i+2}_{\text{soot-H}} + H$	8.0×10^{7}	1.56	3.8	x_{g}
S5	$C^i_{\text{soot-*}} + O_2 \rightarrow 2CO + C^{i-2}_{\text{soot-H}}$	2.2×10^{12}		7.5	x_{O_2}
S6	$C^i_{\text{soot}} + OH \rightarrow CO + C^{i-1}_{\text{soot}}$	reaction probability = 0.13			x_{OH}
S7	$C^i_{\text{soot}} + \text{PAH} \rightarrow C^{i+n_{\text{PAH}}}_{\text{soot}}$	reaction probability = 1.0			x_{cond}

Coagulation refers to the formation of large particles through collision and sticking among the population of soot particles. The process is modelled using the Smoluchowski's equation [51]. The collision frequency is dependent on the Knudsen number. For the collisions occurring under the continuum regime the coagulation kernel is given as

$$\beta^c_{i,j} = x_{\text{cont}} K_c \Big[\frac{1}{i^{1/3}} + \frac{1}{j^{1/3}} + K_c^{'}\Big(\frac{1}{i^{2/3}} + \frac{1}{j^{2/3}}\Big)\Big]\big(i^{1/3} + j^{1/3}\big), \tag{2}$$

and for the collisions under the free-molecular regime the kernel becomes:

$$\beta^f_{i,j} = x_{\text{free}} K_f \Big(\frac{1}{i} + \frac{1}{j}\Big)^{1/2}\big(i^{1/3} + j^{1/3}\big)^2. \tag{3}$$

K_c, $K_c^{'}$ and K_f are the kernel factors which are functions of temperature, gas viscosity and mean free path. x_{cont} and x_{free} are the multipliers used to calibrate the coagulation rates. It is suggested [19] that the collisions of soot particles under Diesel engine conditions are usually in the transition region between the free molecular regime and the continuum regime. Therefore, the harmonic mean value of the coagulation rates determined in the two regimes is adopted as the coagulation rate in this work.

Table 1 lists the mechanism used for soot surface reactions. The soot surface growth is modeled using the HACA mechanism [16]. The oxidation of soot particles via O_2 is described using the concept of soot surface radical sites while the oxidation by OH is modeled through a collision theory between OH radical and soot particles. Condensation is modeled as the deposition of a pyrene molecule from the gas-phase on the surface of soot particles. For all these processes, the multipliers are introduced as listed in Table 1 to tune the corresponding reaction rates.

As already mentioned, these soot particle processes can be modeled by using PBEs. Since the soot particles usually span a wide size range, an infinite number of partial differential equations are needed to describe these processes. In order to reduce the computational cost, the method of moments is adopted to handle the soot model. The moments are

defined as

$$M_r = \sum_{i=i_0}^{\infty} i^r N_i, \quad r = 0, 1, \ldots, \infty, \tag{4}$$

where N_i is the number density of soot particles that contain i carbon atoms. i_0 refers to the smallest particle size. M_r is the r^{th} order moment. The lower-order moments have physical meanings, for example M_0 represents the total soot number and M_1 is related to the total soot mass. One only needs to solve for a few lower-order moments which are sufficient to provide the general information on soot particles. However, the soot moment equations are usually unclosed. The application of the collision kernels leads to the presence of fractional or even negative order moments that are not directly tracked and have to be properly estimated. Another closure problem arises from the soot oxidation process where the number of the smallest soot particles has to be approximated to evaluate the depletion of soot particles. In this work, the Moment Projection Method (MPM) is adopted to handle these problems. The basic idea of MPM is to approximate the PSD with a set of weighted particles and directly track the number of the smallest particles by fixing one of the weighted particle sizes at the smallest size. Please refer to [54, 55] for the detailed numerical algorithm for MPM.

2.3 Integrating the models

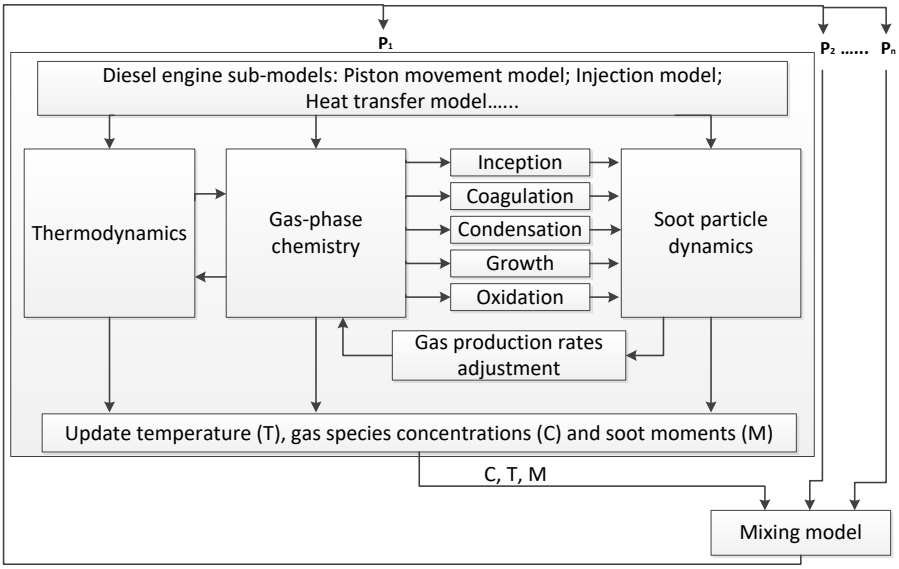

Figure 1: *A schematic of the coupled engine-soot model.*

Figure 1 shows the schematic of the integrated engine-soot model. The engine cylinder charge is split into an ensemble of stochastic particles that represent the distribution of temperature, gas-phase species concentrations and soot moments. The main step of integrating the soot model into the SRM code consists of associating the soot moment equations with each of the SRM stochastic particles and solving them in every computational time step. Another key step is to link the gas-phase chemistry to the soot particle

processes by identifying one or more species in the chemical mechanism as inception and soot surface reaction species. The contributions to these gas-phase species due to soot inception and surface reactions are fed back to the gas-phase chemistry to adjust the corresponding gas species production rates. After these unknowns are updated within each stochastic particle, a mixing among the stochastic particles is conducted to generate new distributions of temperature, gas-phase species concentrations, and soot moments inside the engine cylinder which are fed as inputs into each stochastic particle and repeat the above steps until simulation time ends. It should be noted that the selection of a proper mixing model is very important. An inappropriate mixing of moments may violate the realisability of the moment set, leading to unphysical results. Realisability refers to the existence of an underlying particle size distribution (PSD) which corresponds to a set of moments [9]. All the moments are linked to each other under very complex mathematical relationships. If these relationships are not preserved due to the mixing of moments, the moment set can be unrealisable, indicating that no PSD can be represented by these moments or they lead to unphysical distributions [53]. In this work the mixing of the stochastic particles is described by Curl's model [5] in which a pair of stochastic particles is chosen at a time according to a certain probability law characteristic of the particular model and mixed to produce two new stochastic particles. The properties of the two post-mixed stochastic particles are the mean of the properties of the original ones. Curl's mixing model has been proven in [5] to be able to maintain the consistency between the PSD and the corresponding moments. As a result the realisability of the moment set is ensured.

2.4 Soot model calibration

The seven soot model multipliers described in the previous section were calibrated automatically through MoDS based on the experimental soot emissions obtained at $N = 18$ operating points. The accuracy of the model multipliers was evaluated using a least-squares objective function:

$$f(x) = \sum_{i=1}^{N} \left[\frac{m_i - \widetilde{m}_i(x)}{\sigma_i} \right]^2, \tag{5}$$

where $x = (x_{\text{in}}, x_{\text{cont}}, x_{\text{free}}, x_{\text{g}}, x_{\text{O}_2}, x_{\text{OH}}, x_{\text{cond}})$ refers to the vector of soot model multipliers. m_i and $\widetilde{m}_i$ are, respectively, the experimental and simulated soot emissions for each test case.

The local optimisation was done with the Hooke-Jeeves algorithm [21] which is a type of direct search method. This algorithm is an extension of the basic discrete grid method, both of which are described in [46]. In the basic version, at the k^{th} iteration the algorithm searches for

$$x_k^* \in \mathcal{N}(x_k) : f(x_k^*) < f(x_k), \tag{6}$$

where $\mathcal{N}(x_k)$ is the set of points containing x_k and its immediate neighbours on a grid with spacing δx_k, *i.e.*

$$\mathcal{N}(x_k) = \left\{ x \middle| \exists i \in \{1, \ldots, D\},\ a \in \{-\delta x_k, 0, +\delta x_k\} : x = x_k + a e_i, \right\} \subset \mathbb{R}^D, \tag{7}$$

where e_i is the unit vector in the i^{th} direction, and $D = 7$ in our case. If a better point cannot be found in $\mathcal{N}(x_k)$ then the search distance δx is reduced by multiplying it by $s < 1$. That is, the next point is given by

$$x_{k+1} = \begin{cases} x_k^*, & \text{if } f(x_k^*) < f(x_k), \\ x_k \quad (\text{and } \delta x_{k+1} = s\delta x_k), & \text{otherwise.} \end{cases} \tag{8}$$

Hooke and Jeeves' version extends this by suggesting that if x_k is better than x_{k-1} then taking another step in the same direction to $y_k = 2x_k - x_{k-1}$ and searching for

$$y_k^* \in \mathcal{N}(y_k) : f(y_k^*) < f(x_k), \tag{9}$$

where $\mathcal{N}(y_k)$ is defined as in Eqn. (7), might provide a further improvement. This gives

$$x_{k+1} = \begin{cases} x_k^*, & \text{if } f(x_k^*) < f(x_k) \text{ and } f(y_k^*) \geq f(x_k^*), \\ y_k^*, & \text{if } f(x_k^*) < f(x_k) \text{ and } f(y_k^*) < f(x_k^*), \\ x_k \quad (\text{and } \delta x_{k+1} = s\delta x_k), & \text{otherwise.} \end{cases} \tag{10}$$

The algorithm terminates if either the number of iterations, k, reaches k_{max} or δx_k is reduced such that $\delta x_k < \epsilon$, where ϵ is a user-defined tolerance.

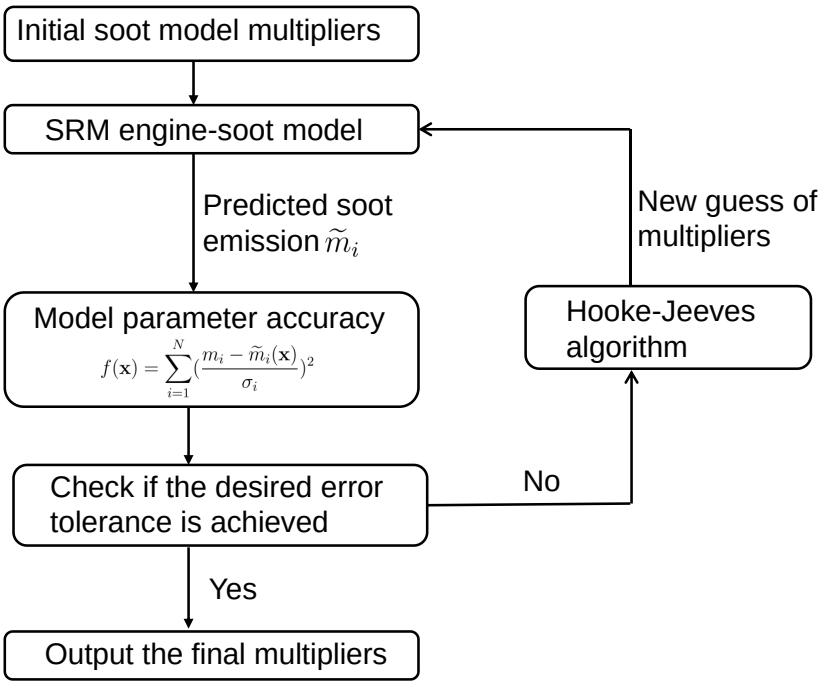

Figure 2: *The calibration workflow for the soot model multipliers in the coupled SRM-MoDS model.*

Figure 2 shows the calibration workflow for the soot model multipliers in the coupled SRM-MoDS model. The values of the multipliers are initially set to 1.0. The predicted

Table 2: *Diesel engine specification.*

Quantity	Value
Bore	105 mm
Stroke	127 mm
Compression ratio	16.5:1
Displacement	4400 cm^3

Table 3: *Engine operating conditions.*

Quantity	Value		Unit
	Min	Max	
Pilot SOI	-18.0	-7.3	CAD ATDC
Main SOI	-10.0	-0.1	CAD ATDC
Main injection fuel mass	100.5	110.0	mg
Injection pressure	1550	2500	bar

soot emissions of the SRM engine-soot model are compared with the experimental measurements to evaluate the accuracy of the soot model multipliers. If the predicted soot emissions are within the user-defined error tolerance, the calibration process stops and outputs the current multipliers as the final results. Otherwise, these multipliers are modified using the Hooke-Jeeves algorithm in order to minimise Eqn. (5). A set of new multipliers are then generated and sent to the SRM engine-soot model to repeat the above procedures until the desired error tolerance for the soot emissions is achieved.

3 Results and discussion

In this section the integrated codes were used to simulate combustion in a four-cylinder, series-turbo-charged heavy-duty Diesel engine from Caterpillar. A detailed kinetic model for Primary Reference Fuel (PRF) [38] is employed to describe the gas phase chemistry. The chemical mechanism contains 208 species and 1002 reactions. The formation of soot precursors including Polycyclic Aromatic Hydrocarbons (PAHs) and other soot surface reaction related species such as acetylene are all included. The simulated Diesel engine has eight valves and a displacement of 4.4 litre with dual injection strategy. Further details of the engine specification are listed in Table 2.

In total 18 test cases were adopted. The range of operating conditions are described in Table 3. The Diesel engine was running at a constant speed of 2200 rpm. The pilot injection fuel mass is always 2.91 mg for all the cases while different injection timings, injection pressures, and main injection fuel mass are adopted. These cases cover a wide range for soot emissions.

For all the cases, simulations were run with a time step of 0.2 CAD. 100 stochastic parti-

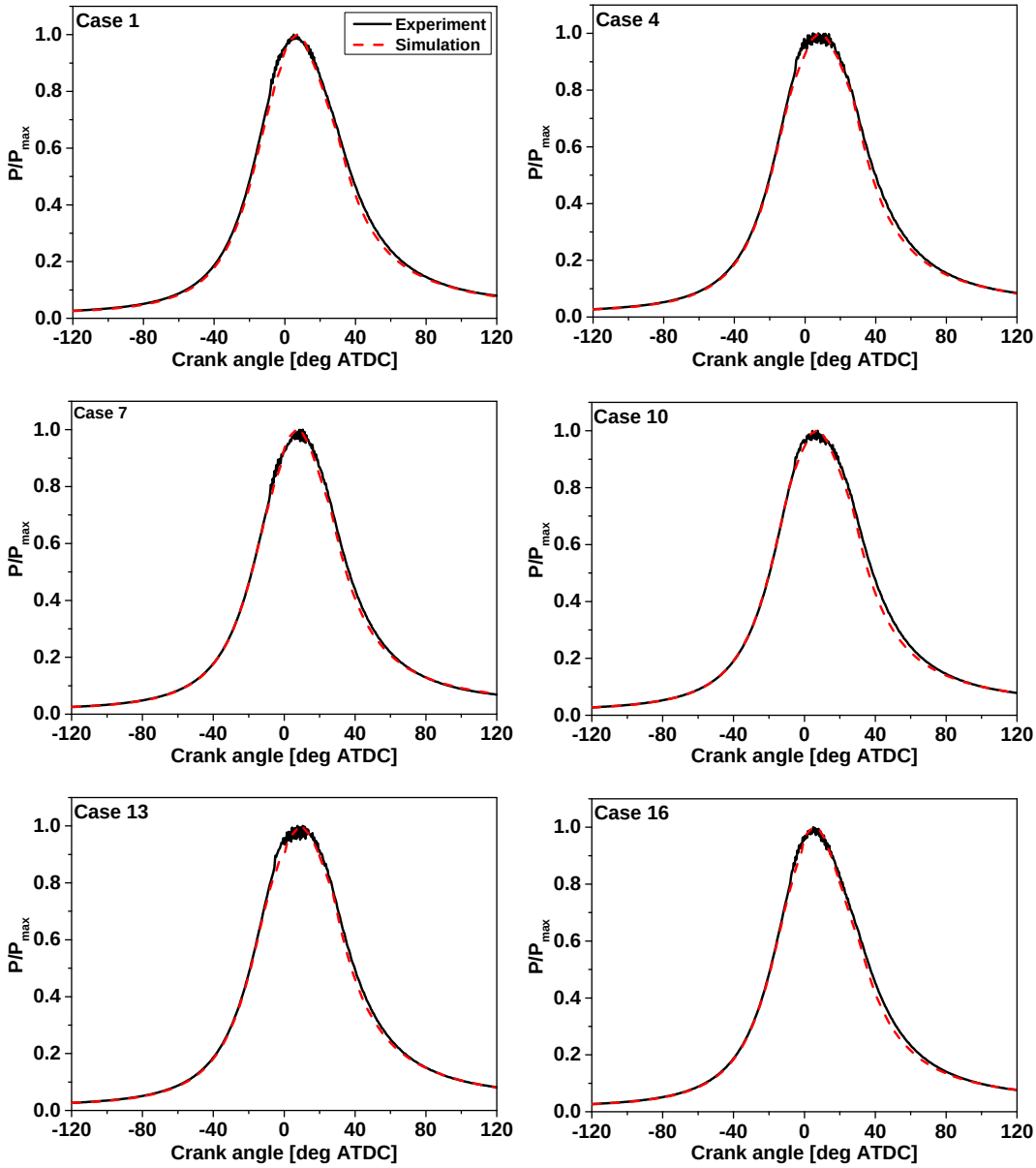

Figure 3: *Comparison between simulated and measured in-cylinder pressures as a function of crank angle. For each case, the pressure values have been normalised by the maximum measured pressure* P_{max}.

cles were adopted in the SRM engine code. Figure 3 compares the simulated in-cylinder pressure profiles with the experimental measurements for six representative test cases. As can be seen the simulation results match the experimental data well. The predicted ignition timings and cumulative heat releases are in good agreement with the experiments. These results suggest that the combustion process inside the Diesel engine cylinder was successfully simulated with the integrated code.

In order to evaluate the computational efficiency of the integrated code for soot simulation in Diesel engines, for each test case the simulation was run twice: one considers both the

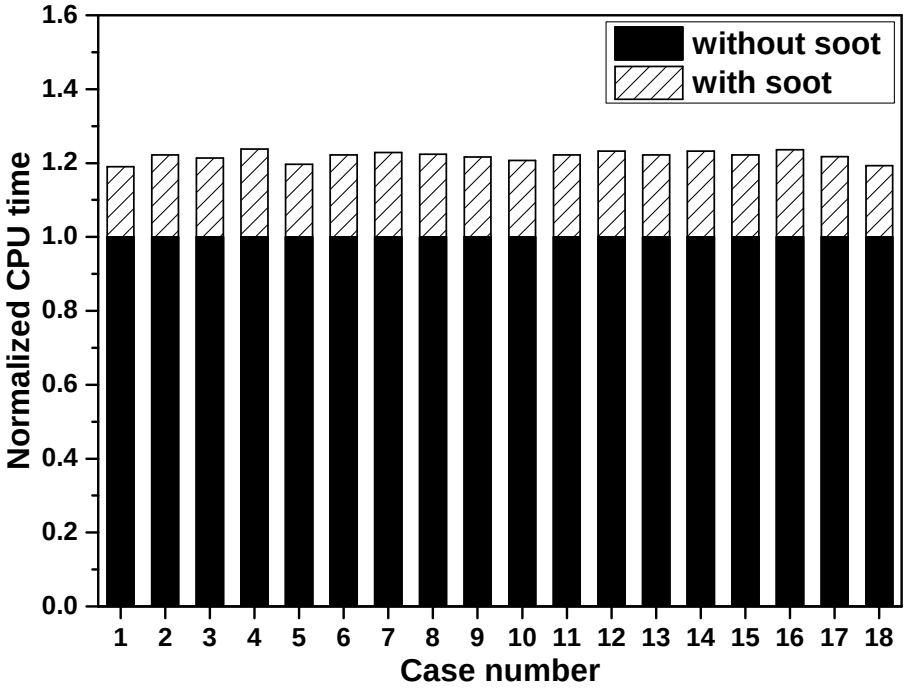

Figure 4: *Evaluation of the additional CPU costs induced by including the soot model in the Diesel engine simulation. For each test case, the CPU time is normalised by the result obtained where no soot particle dynamics are considered.*

gas phase chemistry and the soot particle dynamics while the other one only considers the gas phase chemistry. The CPU time spent for these cases is shown in Fig. 4. Note that for each test case the CPU time is normalised by the result obtained where only gas phase chemistry is considered. As can be seen, the inclusion of the soot model in the code increases the CPU cost by around only 20% for all the test cases owing to the high computational efficiency of MPM. This is very promising given the fact that traditionally the treatment of the soot model using the stochastic method usually makes the Diesel engine simulation prohibitively expensive.

Figure 5 shows the distribution of temperature and equivalence ratio in a plot at several crank angles throughout the cycle for case 1. At CAD = -50, it can be seen that all the stochastic particles are located at a low temperature with a fuel/air equivalence ratio of zero since no fuel has been injected yet and the cylinder has been charged with air. At CAD = -20, these particles are found to be moved to a higher temperature region due to compression while the equivalence ratio still remains zero. Then at CAD = -5 where the pilot injection has already started, the burning of the fuel leads to a fast increase in temperature. Note that the particles with equivalence ratios close to stoichiometric reach the highest temperature as expected. Some stochastic particles start to be present in the NO_x peninsula. As the injection continues, the mixture becomes richer. Starting from Top Dead Center at CAD = 0, some stochastic particles start to enter the soot peninsula and become the source of soot formation. The stochastic particle with the highest equivalence ratio belongs to the area that surrounds the fuel injector where very little air exists. During the main combustion period from CAD = 0 to CAD = 30, the stochastic particles span a

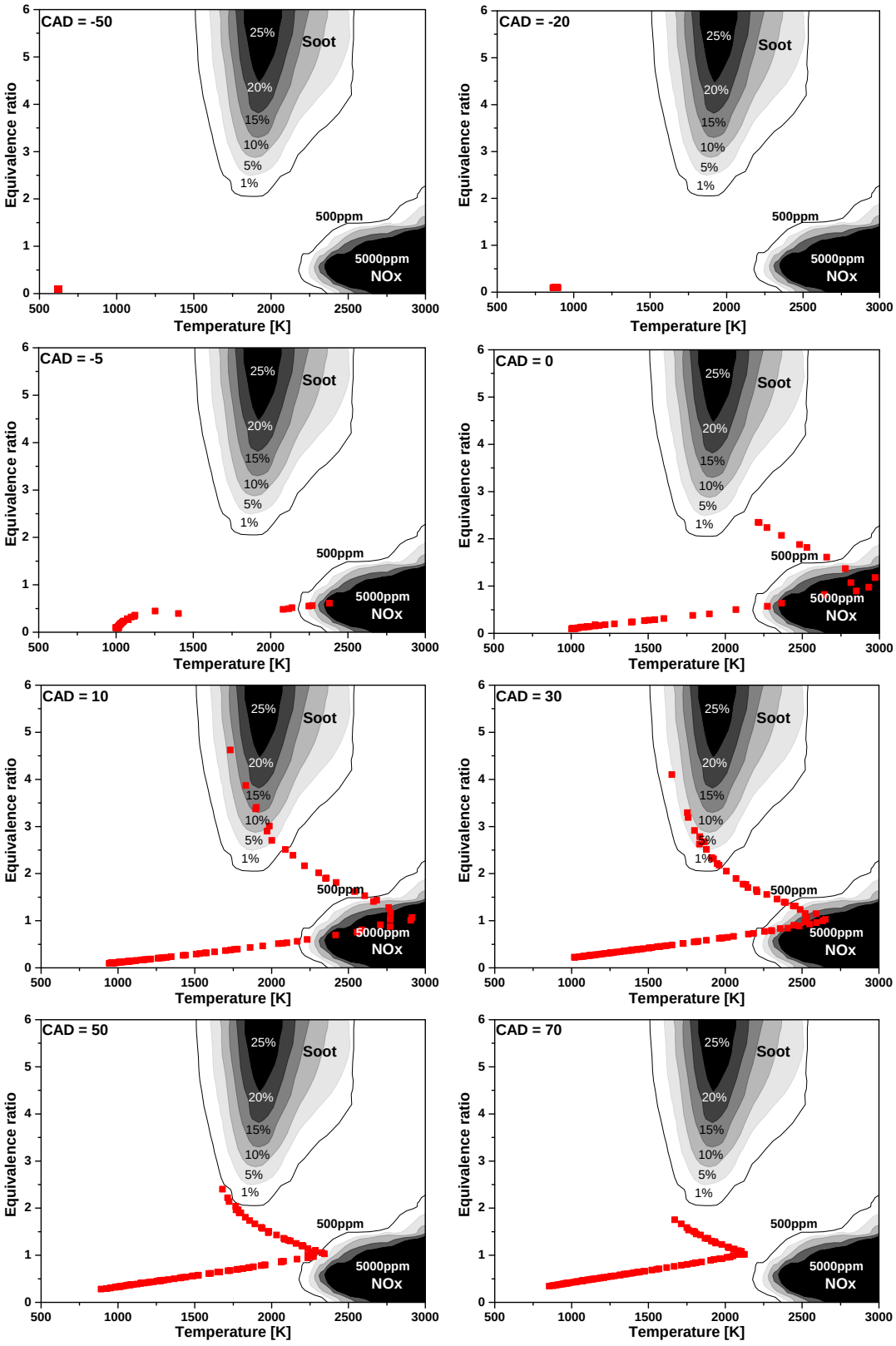

Figure 5: *Time evolution of equivalence ratio and temperature distribution as a function of crank angle for case 1 obtained using the integrated code. The soot and NO_x iso-lines are adopted from [22].*

wide range of equivalence ratios and temperatures, leading to the continuous formation of both NO_x and soot. Then from CAD = 50, a shift of these stochastic particles towards lower temperature and smaller equivalence ratio is observed as the fuel is burned out. These particles start to leave the soot and NO_x peninsula. The formation rates for soot and NO_x are expected to decrease.

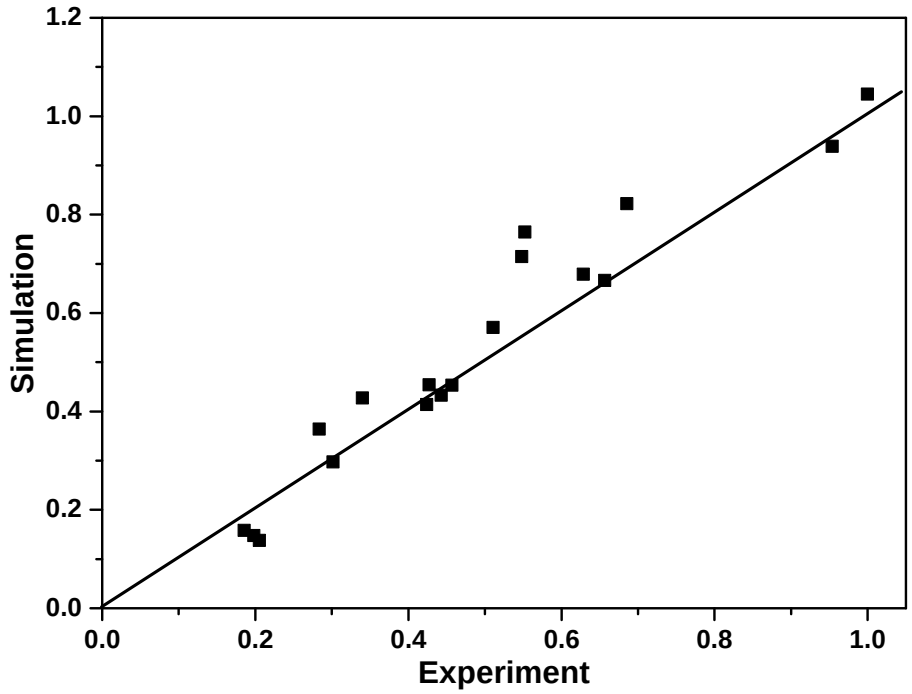

Figure 6: *Comparison between the simulation results and experimental measurements for NO_x emissions for the 18 test cases. Values are normalised by the maximum experimental NO_x emission value. The solid line indicates a 1:1 relation.*

The simulation results and experimental measurements for NO_x and soot emissions are compared in Figs. 6 and 7, respectively. As can be seen the predicted NO_x emissions by the integrated code are in good agreement with the experimental measurements both qualitatively and quantitatively for all 18 test cases. By contrast, the soot emissions are largely over-predicted by the uncalibrated soot model where all the soot process multipliers are set as 1.0. This indicates that the formation and growth rates for soot particles under Diesel engine combustion conditions have been overestimated with the original soot model parameters.

The calibration of the soot model multipliers was completed after 156 simulation runs. The finally accepted multipliers determined by the Hooke-Jeeves algorithm are shown in Fig. 8. It can be seen that only the multipliers for soot surface growth, oxidation via molecular oxygen and free-molecular coagulation are changed significantly while the multipliers for other soot particle processes remain almost unchanged. In particular, x_{free} has been increased by around 327 times. The predicted soot emissions with the calibrated soot model are compared with the uncalibrated results and the experimental data in Fig. 7. A much better agreement between the simulation results and the experimental measurements is observed with the calibrated soot model compared with the uncalibrated one,

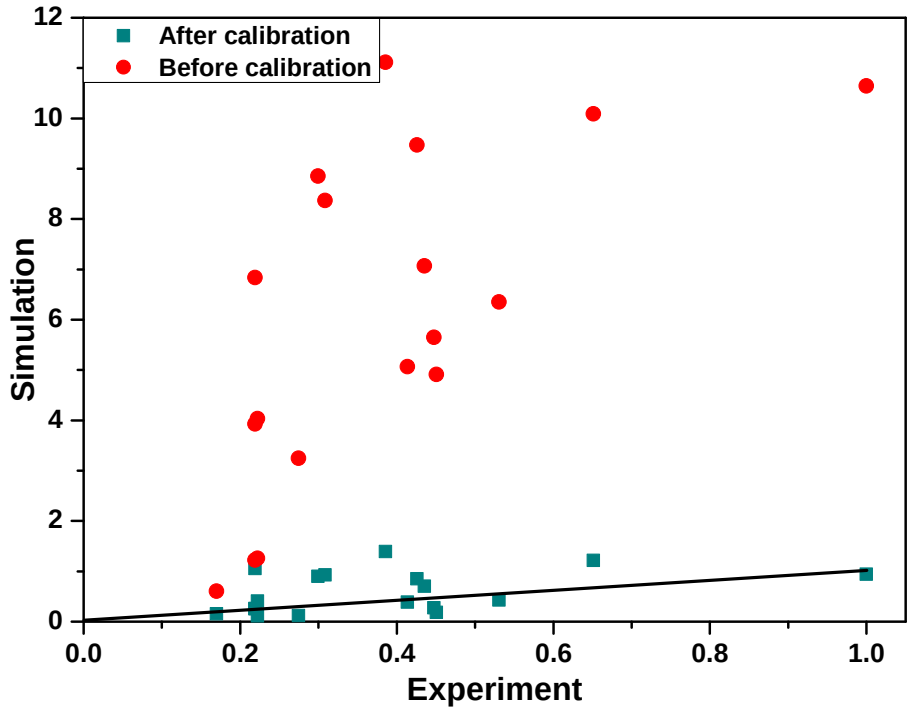

Figure 7: *Comparison between the experimental soot mass and the simulated results before and after calibration of soot model parameters. Values are normalised by the maximum experimental value for the soot emission. The solid line indicates a 1:1 relation.*

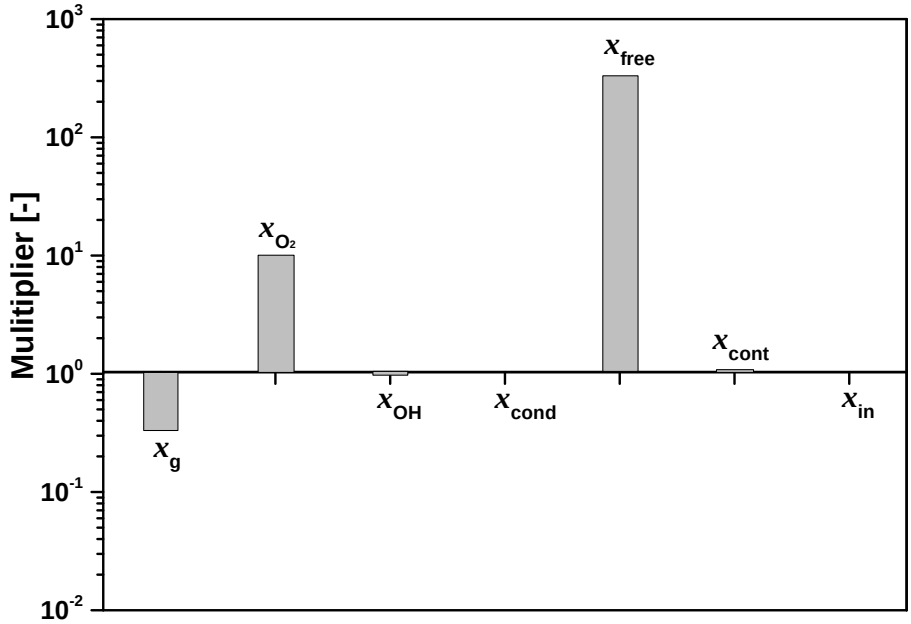

Figure 8: *Change of the soot model multipliers after calibration.*

suggesting that the soot formation rates have been tuned to be more reasonable. However,

in Fig. 7 we could still observe some discrepancies between the experimental measurements and the simulation results obtained with the calibrated soot model. For example the soot emissions in cases 2, 4, 8, 10, and 12 are over-predicted by around two orders with the new multipliers. These discrepancies might be a consequence of the inherent defects of the adopted soot model for describing the soot formation and oxidation processes. The detailed soot formation mechanism is far from being fully understood. Take inception as an example, the inception mechanism adopted in the current soot model is a very simple one which assumes the pyrene molecule to be the only soot precursor. The inception rate is determined through a simple collision equation. However, several studies [2, 56] indicate that PAHs larger than pyrene might act as the soot inception species. Furthermore, it has been suggested that the soot inception process should be reversible which is not the case in the adopted soot model. A better agreement between the experimental data and the simulation results can be expected if a more accurate soot model is adopted. It should be noted that the purpose of this paper is not to develop a new soot model but to present an efficient calibration procedure for soot simulation in Diesel engines. The proposed engine-soot model in this work has the advantage of low computational cost. The soot model multipliers have been successfully calibrated via the coupled SRM-MoDS code.

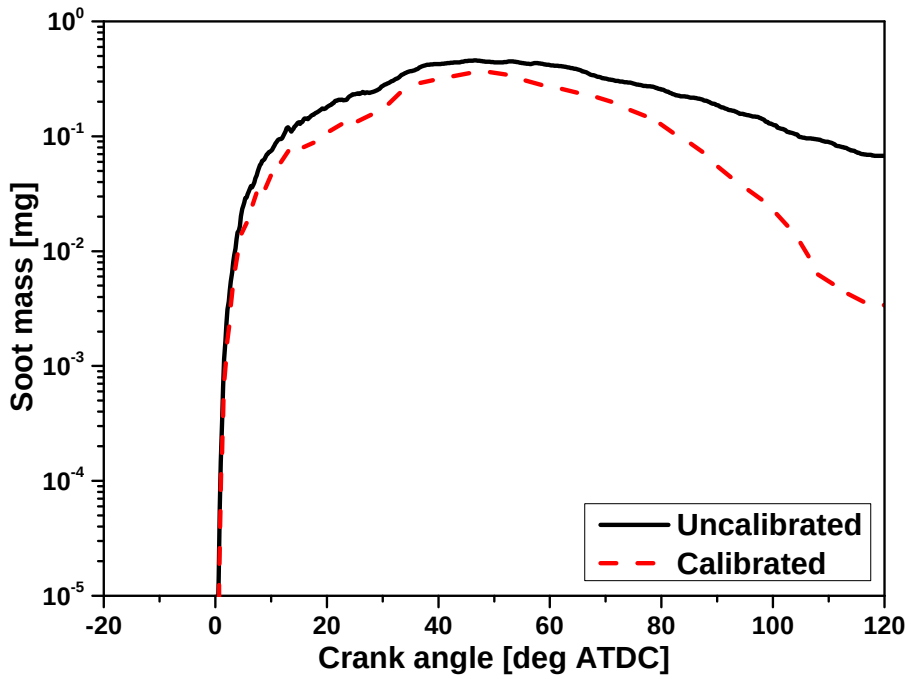

Figure 9: *Comparison of the time evolution of the total soot mass as a function of crank angle obtained before and after calibration of the soot model for case 1.*

Next, the influence of the soot model multipliers on the soot formation and oxidation processes are discussed. Figure 9 compares the time evolution of the predicted total soot mass as a function of crank angle for case 1 obtained before and after the calibration of the soot model multipliers. As can be seen, at the beginning inception dominates the soot particle processes, leading to a fast build-up of soot mass inside the engine cylinder. The total soot mass keeps increasing until around CAD = 50 after which oxidation starts to dominate over the soot formation process. During the whole combustion process less

soot mass is predicted using the calibrated soot model compared with the original one. Especially during the late combustion stage the soot mass predicted with the calibrated soot model exhibits a sharp decrease while the uncalibrated model leads to a slow change of the soot mass.

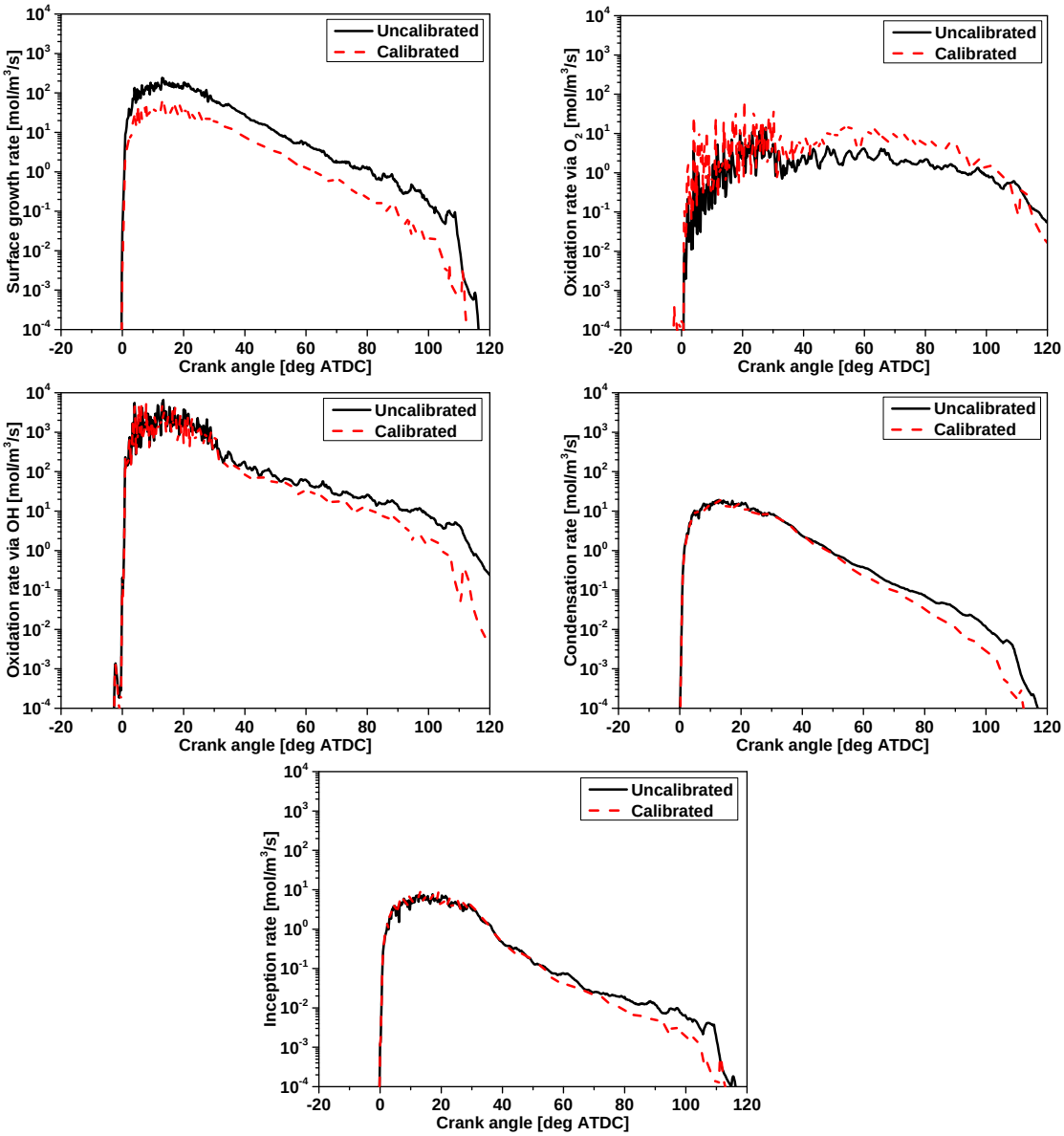

Figure 10: *Time evolution of the soot inception and surface reaction rates as a function of crank angle for case 1 obtained using the integrated code.*

The predicted soot formation and oxidation rates for case 1 obtained before and after calibration of the soot model are shown in Fig. 10. The coagulation rate for the total soot mass is zero, therefore it is not shown in the figure. From Fig. 10 it can be seen that the oxidation rate via OH is much larger than that via O_2, suggesting that the soot oxidation process is mainly governed by the external burning process. During the main combustion stage from 0 CAD to 60 CAD, the soot inception rates, condensation rates

and surface oxidation rates predicted by the calibrated and uncalibrated soot models are almost the same. By contrast, the calibrated soot model leads to a lower soot surface growth rate compared with the uncalibrated model, which is the main contributor for the less soot mass obtained by the calibrated soot model as observed in Fig. 9. During the late combustion stage ($>$ 60 CAD), the calibrated soot model predicts a lower rate for not only the surface growth but also the inception and condensation processes compared with the uncalibrated soot model, which leads to a faster decrease in the total soot mass as observed in Fig. 9.

One significant weakness of the method of moments is that it can only provide the bulk quantities of soot particles while the detailed soot PSD is lost. In order to perform a comprehensive study on the soot particle dynamics, the maximum entropy (ME) approach [35] is adopted in this work as a post-process technique to reconstruct the soot PSD based on the obtained moments at each simulation step. The basic idea of ME reconstruction is to approximate the PSD using a series of exponential polynomials, which is given as

$$N(i) = \exp\Big(- \sum_{j=0}^{K} \lambda_j i^j \Big), \tag{11}$$

where λ_j ($j = 0, \ldots, K$) are Lagrange multipliers. The reconstructed PSD has to meet the requirement that the first $K + 1$ moments are equal to the moments of the real PSD:

$$\sum_{i=i_{\min}}^{i_{\max}} i^r N_K(i) = \sum_{i=i_{\min}}^{i_{\max}} i^r \exp\Big(- \sum_{j=0}^{K} \lambda_j i^j \Big) = M_r, \quad r = 0, \ldots, K. \tag{12}$$

The key problem is to determine these Lagrange multipliers. To achieve this, a convex potential is introduced:

$$\Delta = \sum_{i=i_{\min}}^{i_{\max}} \Big[\exp\Big(- \sum_{j=0}^{K} \lambda_j i^j \Big) - 1 \Big] + \sum_{j=0}^{K} M_j \lambda_j. \tag{13}$$

One just needs to minimise this potential to find its stationary points. Please refer to [35] for the detailed ME algorithm.

The reconstructed soot PSDs as a function of crank angle for case 1 obtained before and after calibration of the soot model multipliers are compared in Fig. 11. As can be seen, at the beginning inception dominates the soot formation process, the PSD exhibits a delta distribution. An increase in the total soot number is observed from CAD = -5 to CAD = 0 as injection continues. From CAD = 4, the soot PSD starts to exhibit a bimodal distribution. The first mode arises from the continuous particle inception while the second mode is due to the particle growth and coagulation processes. As more and more particles are formed, the PSD is becoming wider. At the same time, the inception process is weakened as most fuels have been burned out and a shift of the PSD from bimodal to unimodal distribution is observed at the late combustion stage accompanied by a continuous decrease of the total soot number. Compared with the uncalibrated soot model, the calibrated soot model predicts a narrower soot PSD during the main combustion period from CAD = 4 to CAD = 35. This is mainly attributed to the decrease in the soot surface growth multiplier

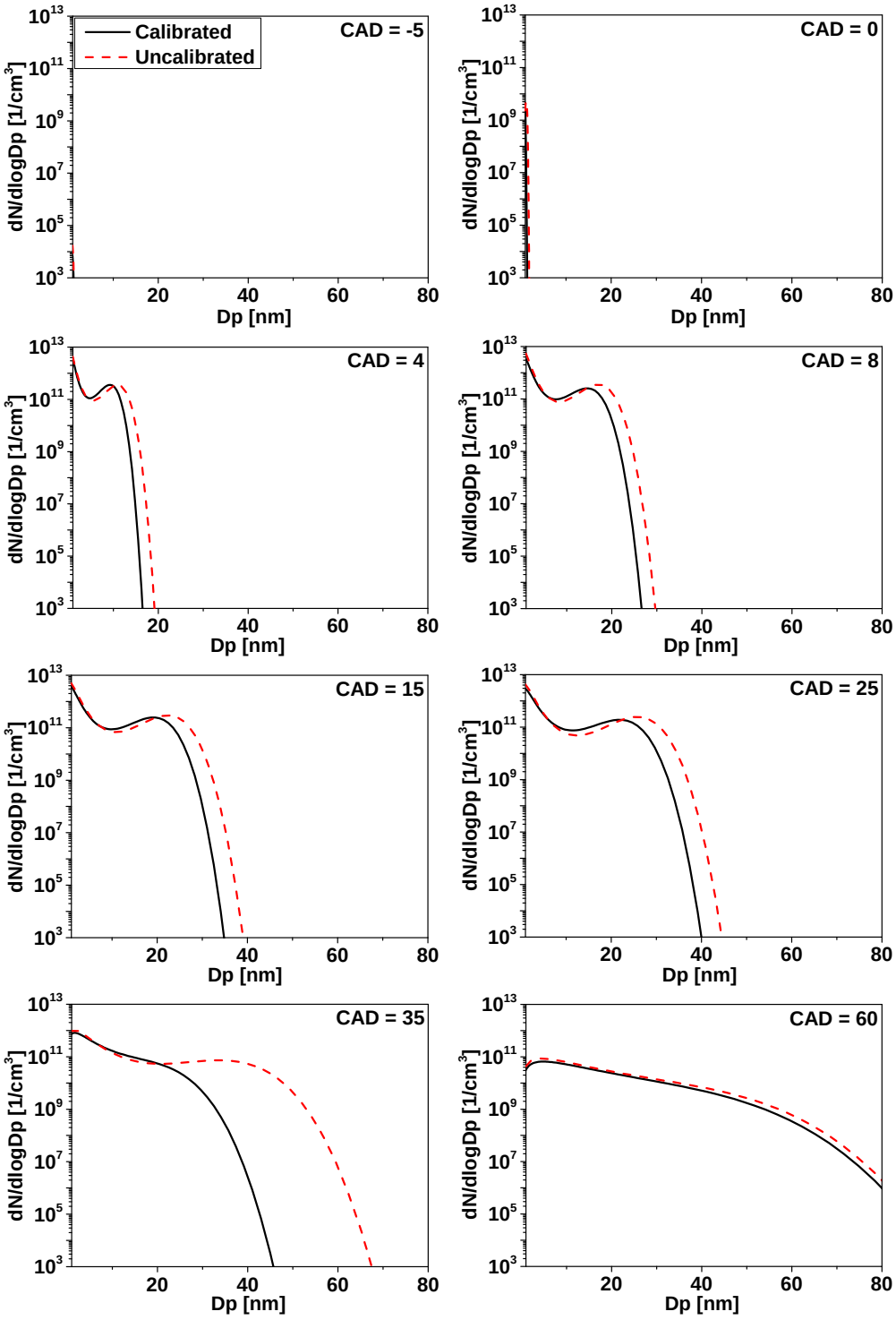

Figure 11: *Predicted time evolution of the soot particle size distributions for case 1 obtained before and after calibration of the soot model multipliers.*

after calibration, which leads to a slow accumulation of soot particles at large sizes. In addition, the increase of the soot oxidation multiplier after calibration results in an overall lower soot number through the whole particle size range compared with the uncalibrated

soot model. During the late combustion stage, the coagulation process starts to dominate the particle process as the soot surface reactions become weakened. Since the coagulation multiplier has been increased after calibration, a faster increase in the soot particle size range is induced by the calibrated soot model compared with the uncalibrated one.

The predicted evolution of the soot PSD within the engine cylinder seems reasonable. Unfortunately there is no available experimental measurement for engine in-cylinder soot PSD for comparison. Once again, it should be noted that the purpose of this paper is not to develop a new soot model to account for the soot formation and oxidation processes precisely. The aim here is to present an efficient approach for soot simulation in Diesel engines over a wide range of operating conditions. The integrated code proposed here can be used to handle the soot model with little CPU cost. It enables an auto-calibration of the model parameters which represents a significant improvement over the manual calibration which is time-consuming and impractical. Furthermore, a detailed analysis on the soot particle evolution inside the engine cylinder can be provided.

4 Conclusion

In this work, a calibration procedure for soot simulation in Diesel engines is developed and presented. The procedure is based on the integration between the engine-soot model and an advanced optimisation method. The Stochastic Reactor Model (SRM) engine code is adopted to describe the combustion process inside Diesel engines. The Moment Projection Method (MPM) is implemented into SRM to account for the soot particle dynamics including inception, condensation, coagulation, surface growth, and oxidation. The SRM code is then coupled with the Model Development Suite (MoDS) where the Hooke-Jeeves algorithm is adopted for the automatic calibration of the soot model parameters based on the experimental measurements for soot emissions.

The performance of the integrated code has been tested by simulating the soot formation and oxidation processes in a four-cylinder heavy-duty Diesel engine operated under 18 different conditions which cover a wide range for soot emissions. Results suggest that the integrated code is very efficient. The inclusion of the soot model in the engine code leads to an increase of CPU cost by only around 20%. The auto-calibration of the soot model parameters is completed after 144 simulation runs. A much better agreement between the simulation results and the measured soot emissions is achieved with the calibrated soot model compared to the original one, suggesting that the Hooke-Jeeves algorithm successfully finds the desired parameters. It is found that the major changes to the soot model parameters after calibration are the surface growth multiplier, O_2 oxidation multiplier, and free-molecular coagulation multiplier. A detailed investigation on the influences of these multipliers on the soot formation and oxidation processes in Diesel engines is provided. With the integrated code, not only the bulk soot quantities such as total soot number and mass but also the evolution of the detailed soot PSDs can be generated, enabling a comprehensive study on the soot particle dynamics in Diesel engines.

Acknowledgements

This work was partly funded by the National Research Foundation (NRF), Prime Minister's Office, Singapore under its Campus for Research Excellence and Technological Enterprise (CREATE) programme, and by the Advanced Propulsion Centre UK in the framework of APC3 Project 113059 - ASCENT (Advanced Systems for Carbon Emission reduction through New Technology). Markus Kraft gratefully acknowledges the support of the Alexander von Humboldt foundation.

Nomenclature

Upper-case Roman

A	Pre-exponential factor
C	Gas species concentration
E	Activation energy
K	Kernel
M	Moment
N	Number
P	Pressure
R	Universal gas constant
T	Temperature

Lower-case Roman

e	Unit vector
k	Rate constant
k_{B}	Boltzmann constant
r_i	Radius of particle of size i
m	Mass
x	Multiplier

Greek

β	Collision kernel
Δ	Convex potential
ϵ	Tolerance
ε	Enhancement factor
λ	Lagrange multiplier
μ	Reduced mass

Superscripts

g	Gas

c	Continuum regime
f	Free-molecular regime

Symbols

$\widetilde{x}$	Approximation of x
x^*	New guess of x

Abbreviations

CAD	Crank angle degree
EOI	End of injection
EVC	Exhaust valve closing
EVO	Exhaust valve opening
GA	Genetic algorithm
HACA	Hydrogen abstraction and acetylene addition
HCM	Hybrid calibration method
ICE	Internal combustion engine
IVC	Inlet valve closing
IVO	Inlet valve opening
ME	Maximum entropy
MoDS	Model development suite
MOM	Method of moments
MPM	Moment projection method
OPAL	Optimisation algorithm
PAH	Polycyclic aromatic hydrocarbon
PBE	Population balance equation
PDF	Probability density function
PM	Particulate matter
PRF	Primary reference fuel
PSD	Particle size distribution
SOI	Start of injection
SRM	Stochastic reactor model

References

[1] V. Alopaeus, M. Laakkonen, and J. Aittamaa. Solution of population balances with breakage and agglomeration by high-order moment-conserving method of classes. *Chem. Eng. Sci.*, 61(20):6732–6752, 2006. doi:10.1016/j.ces.2006.07.010.

[2] J. Appel, H. Bockhorn, and M. Frenklach. Kinetic modeling of soot formation with detailed chemistry and physics: Laminar premixed flames of C_2 hydrocarbons. *Combust. Flame.*, 121(1–2):122–136, 2000. doi:10.1016/S0010-2180(99)00135-2.

[3] M. Balthasar and M. Frenklach. Detailed kinetic modeling of soot aggregate formation in laminar premixed flames. *Combust. Flame*, 140:130–145, 2005. doi:10.1016/j.combustflame.2004.11.004.

[4] M. Balthasar and M. Kraft. A stochastic approach to calculate the particle size distribution function of soot particles in laminar premixed flames. *Combust. Flame*, 133(3):289–298, 2003. doi:10.1016/S0010-2180(03)00003-8.

[5] M. Balthasar, F. Mauss, A. Knobel, and M. Kraft. Detailed Modeling of Soot Formation in a Partially Stirred Plug Flow Reactor. *Combust. Flame.*, 128:395–409, 2002. doi:10.1016/S0010-2180(01)00344-3.

[6] M. Bolla, D. Farrace, Y. M. Wright, and K. Boulouchos. Modelling of soot formation in a heavy-duty diesel engine with conditional moment closure. *Fuel*, 117:309–325, 2014. doi:10.1016/j.fuel.2013.09.041.

[7] J. Boulanger, F. Liu, W. S. Neill, and G. J. Smallwood. An improved soot formation model for 3D diesel engine simulations. *J. Eng. Gas Turb. Power.*, 129:877–884, 2007. doi:10.1115/1.2718234.

[8] G. P. E. Brownbridge, A. J. Smallbone, W. Phadungsukanan, M. Kraft, and B. Johansson. Automated IC engine model development with uncertainty propagation. *SAE Technical Paper No. 2011-01-0237*, 2011. doi:10.4271/2011-01-0237.

[9] A. Buffo, M. Vanni, and D. L. Marchisio. On the implementation of moment transport equations in OpenFOAM: Boundedness and realizability. *Int. J. Multiph. Flow.*, 85:223–235, 2016. doi:10.1016/j.ijmultiphaseflow.2016.06.017.

[10] R. B. Diemer and J. H. Olson. A moment methodology for coagulation and breakage problems: part 2 – moment models and distribution reconstruction. *Chem. Eng. Sci.*, 57(12):2211–2228, 2002. doi:10.1016/S0009-2509(02)00112-4.

[11] K. Donaldson, L. Tran, L. A. Jimenez, R. Duffin, D. E. Newby, N. Mills, W. MacNee, and V. Stone. Combustion-derived nanoparticles: A review of their toxicology following inhalation exposure. *Part. Fibre Toxicol.*, 2:1–14, 2005. doi:10.1186/1743-8977-2-10.

[12] P. Eastwood. *Particulate emissions from vehicles*. John Wiley, 2008.

[13] J. Etheridge, S. Mosbach, M. Kraft, H. Wu, and N. Collings. Modelling soot formation in a DISI engine. *Proc. Combust. Inst.*, 33:3159–3167, 2011. doi:10.1016/j.proci.2010.07.039.

[14] V. Fraioli, C. Beatrice, and M. Lazzaro. Soot particle size modelling in 3D simulations of diesel engine combustion. *Combust. Theor. Model.*, 15:863–892, 2011. doi:10.1080/13647830.2011.578662.

[15] M. Frenklach. Method of moments with interpolative closure. *Chem. Eng. Sci.*, 57 (12):2229–2239, 2002. doi:10.1016/S0009-2509(02)00113-6.

[16] M. Frenklach and H. Wang. Detailed modeling of soot particle nucleation and growth. *Proc. Combust. Inst.*, 23:1559–1566, 1991. doi:10.1016/S0010-2180(99)00135-2.

[17] H. Hiroyasu and T. Kadota. Models for Combustion and Formation of Nitric Oxide and Soot in Direct Injection Diesel Engines. *SAE Technical Paper No. 760129*, 1976. doi:10.4271/760129.

[18] H. Hiroyasu and K. Nishida. Simplified three-dimensional modeling of mixture formation and combustion in D. I. diesel engine. *SAE Technical Paper No. 890269*, 1989. doi:10.4271/890269.

[19] S. Hong, M. S. Wooldridge, H. G. Im, D. N. Assanis, and H. Pitsch. Development and application of a comprehensive soot model for 3D CFD reacting flow studies in a diesel engine. *Combust. Flame.*, 143:11–26, 2005. doi:10.1016/j.combustflame.2005.04.007.

[20] S. Hong, M. S. Wooldridge, H. G. Im, D. N. Assanis, and E. Kurtz. Modeling of diesel combustion, soot and NO emissions based on a modified eddy dissipation concept. *Combust. Sci. and Tech.*, 180:1421–1448, 2008. doi:10.1080/00102200802119340.

[21] R. Hooke and T. A. Jeeves. "Direct Search" solution of numerical and statistical problems. *J. ACM*, 8:212–229, 1961. doi:10.1145/321062.321069.

[22] T. Kamimoto and M. Bae. Combustion temperature for the reduction of particulate in diesel engines. *SAE Technical Paper No. 880423*, 1988. doi:10.4271/880423.

[23] A. Kazakov and D. Foster. Modeling of soot formation during DI diesel combustion using multistep phenomenological model. *SAE Technical Paper No. 982463*, 1998. doi:10.4271/982463.

[24] A. Kazakov and M. Frenklach. Dynamic modeling of soot particle coagulation and aggregation: implementation with the method of moments and application to high–pressure laminar premixed flames. *Combust. Flame*, 114:484–501, 1998. doi:10.1016/S0010-2180(97)00322-2.

[25] D. B. Kittelson. Engines and nanoparticles: a review. *J. Aerosol Sci.*, 29:575–588, 1998. doi:10.1016/S0021-8502(97)10037-4.

[26] M. Kraft, P. Maigaard, F. Mauss, M. Christensen, and B. Johansson. Investigation of combustion emissions in a homogeneous charge compression injection engine: Measurements and a new computational model. *Proc. Combust. Inst.*, 28(1):1195–1201, 2000. doi:10.1016/S0082-0784(00)80330-6.

[27] S. Kumar and D. Ramkrishna. On the solution of population balance equations by discretization – I. A fixed pivot technique. *Chem. Eng. Sci.*, 51(8):1311–1332, 1996. doi:10.1016/0009-2509(96)88489-2.

[28] S. Kumar and D. Ramkrishna. On the solution of population balance equations by discretization – II. A moving pivot technique. *Chem. Eng. Sci.*, 51(8):1333–1342, 1996. doi:10.1016/0009-2509(95)00355-X.

[29] J. Lai, O. Parry, S. Mosbach, and A. Bhave. Evaluating emissions in a modern compression ignition engine using multi-dimensional PDF-based stochastic simulations and statistical surrogate generation. *SAE Technical Paper No. 2018-01-1739*, 2018. doi:10.4271/2018-01-1739.

[30] K. F. Lee, R. I. A. Patterson, W. Wagner, and M. Kraft. Stochastic weighted particle methods for population balance equations with coagulation, fragmentation and spatial inhomogeneity. *J. Comput. Phys.*, 303:1–18, 2015. doi:10.1016/j.jcp.2015.09.031.

[31] E. Madadi-Kandjani and A. Passalacqua. An extended quadrature-based moment method with log-normal kernel density functions. *Chem. Eng. Sci.*, 131:323–339, 2015. doi:10.1016/j.ces.2015.04.005.

[32] M. Massot, F. Laurent, D. Kah, and S. D. Chaisemartin. A robust moment method for evaluation of the disappearance rate of evaporating sprays. *Siam J. Appl. Math.*, 70:3203–3234, 2010. doi:10.1137/080740027.

[33] F. Mauss, T. Schäfer, and H. Bockhorn. Inception and growth of soot particles in dependence on the surrounding gas phase. *Combust. Flame*, 99:697–705, 1994. doi:10.1016/0010-2180(94)90064-7.

[34] R. McGraw. Description of aerosol dynamics by the quadrature method of moments. *Aerosol Sci. Tech.*, 27(2):255–265, 1997. doi:10.1080/02786829708965471.

[35] L. R. Mead and N. Papanicolaou. Maximum entropy in the problem of moments. *J. Math. Phys.*, 25:2404–2417, 1984. doi:10.1063/1.526446.

[36] P. Mitchell and M. Frenklach. Particle aggregation with simultaneous surface growth. *Phys. Rev. E*, 67:1–11, 2003. doi:10.1103/PhysRevE.67.061407.

[37] S. Mosbach, H. Su, M. Kraft, A. Bhave, F. Mauss, Z. Wang, and J.-X. Wang. Dual injection homogeneous charge compression ignition engine simulation using a stochastic reactor model. *Int. J. Engine Res.*, 8(1):41–50, 2007. doi:10.1243/14680874JER01806.

[38] S. Mosbach, M. S. Celnik, A. Raj, M. Kraft, H. R. Zhang, S. Kubo, and K. O. Kim. Towards a detailed soot model for internal combustion engines. *Combust. Flame.*, 156:1156–1165, 2009. doi:10.1016/j.combustflame.2009.01.003.

[39] S. Mosbach, A. Braumann, P. L. W. Man, C. A. Kastner, G. P. E. Brownbridge, and M. Kraft. Iterative improvement of Bayesian parameter estimates for an engine model by means of experimental design. *Combust. Flame*, 159:1303–1313, 2012. doi:10.1016/j.combustflame.2011.10.019.

[40] M. E. Mueller, G. Blanquart, and H. Pitsch. Hybrid method of moments for modelling soot formation and growth. *Combust. Flame.*, 156:1143–1155, 2009. doi:10.1016/j.combustflame.2009.01.025.

[41] Q. Y. Niu, C. Fan, C. Wang, Y. W. Zhao, and Y. C. Dong. Research on the parameter calibration of the internal combustion engine work process simulation model. *Adv. Mat. Res.*, 308–310:953–961, 2011. doi:10.4028/www.scientific.net/AMR.308-310.953.

[42] O. Parry, J. Dizy, V. Page, A. Bhave, and D. Ooi. Fast response surrogates and sensitivity analysis based on physico-chemical engine simulation applied to modern compression ignition engines. *IAV International Calibration Conference, May 11-12, 2017, Berlin*, 2017.

[43] M. Pasternak, F. Mauss, G. Janiga, and D. Thévenin. Self-calibrating model for diesel engine simulations. *SAE Technical Paper No. 2012-01-1072*, 2012. doi:10.4271/2012-01-1072.

[44] M. Pasternak, F. Mauss, C. Perlman, and H. Lehtiniemi. Aspects of 0D and 3D modeling of soot formation for diesel engines. *Combust. Sci. Technol.*, 186:1517–1535, 2014. doi:10.1080/00102202.2014.935213.

[45] S. B. Pope. PDF methods for turbulent reactive flows. *Prog. Energy Combust. Sci.*, 11:119–192, 1985. doi:10.1016/0360-1285(85)90002-4.

[46] M. J. D. Powell. Direct search algorithms for optimization calculations. *Acta Numer.*, 7:287–336, 1998. doi:10.1017/S0962492900002841.

[47] I. Prah, F. Trenc, and T. Katrašnik. Innovative calibration method for system level simulation models of internal combustion engines. *Energies*, 9, 2016. doi:10.3390/en9090708.

[48] D. Ramkrishna. *Population Balances: Theory and Applications to Particulate Systems in Engineering*. Academic Press, New York, 2000.

[49] C. A. Schuetz and M. Frenklach. Nucleation of soot: molecular dynamics simulations of pyrene dimerization. *Proc. Combust. Inst.*, 29:2307–2314, 2002. doi:10.1016/S1540-7489(02)80281-4.

[50] F. Tao, R. D. Reitz, D. E. Foster, and Y. Liu. Nine-step phenomenological diesel soot model validated over a wide range of engine conditions. *Int. J. Therm. Sci.*, 48:1223–1234, 2009. doi:10.1016/j.ijthermalsci.2008.08.014.

[51] M. von Smoluchowski. Versuch einer mathematischen Theorie der Koagulationskinetik kolloider Lösungen. *Z. Phys. Chem.*, 92U:129–168, 1917. doi:10.1515/zpch-1918-9209.

[52] B. Wang, S. Mosbach, S. Schmutzhard, S. Shuai, Y. Huang, and M. Kraft. Modelling soot formation from wall films in a gasoline direct injection engine using a detailed population balance model. *Appl. Energy*, 163:154–166, 2016. doi:10.1016/j.apenergy.2015.11.011.

[53] D. L. Wright Jr. Numerical advection of moments of the particle size distribution in Eulerian models. *J. Aerosol Sci.*, 38:352–369, 2007. doi:10.1016/j.jaerosci.2006.11.011.

[54] S. Wu, E. K. Y. Yapp, J. Akroyd, S. Mosbach, R. Xu, W. Yang, and M. Kraft. A moment projection method for population balance dynamics with a shrinkage term. *J. Comput. Phys.*, 330:960–980, 2017. doi:10.1016/j.jcp.2016.10.030.

[55] S. Wu, E. K. Y. Yapp, J. Akroyd, S. Mosbach, R. Xu, W. Yang, and M. Kraft. Extension of moment projection method to the fragmentation process. *J. Comput. Phys.*, 335:516–534, 2017. doi:10.1016/j.jcp.2017.01.045.

[56] Y. Wang, A. Raj, S.H. Chung. A PAH growth mechanism and synergistic effect on PAH formation in counterflow diffusion flames. *Combust. Flame*, 160:1667–1676, 2013. doi:10.1016/j.combustflame.2013.03.013.

[57] C. Yuan, F. Laurent, and R. O. Fox. An extended quadrature method of moments for population balance equations. *J. Aerosol Sci.*, 51:1–23, 2012. doi:10.1016/j.jaerosci.2012.04.003.